

Effects of glissile interstitial clusters on microstructure self-organization in irradiated materials

D. Walgraef¹ and N. M. Ghoniem²

¹*Center of Nonlinear Phenomena and Complex Systems, Free University of Brussels, Case Postale 231, Bd du Triomphe, B-1050 Brussels, Belgium*

²*Mechanical and Aerospace Engineering Department, The University of California at Los Angeles, Los Angeles, California 90024*

(Received 01 August 2002; revised manuscript received 18 November 2002)

We analyze the formation and selection of self-organized defect microstructure in irradiated materials within the framework of a kinetic model for point and clustered defects. We take explicitly into account the influence of glissile interstitial clusters on the stability and morphology of ordered microstructure. Under void growth conditions, we find that the anisotropic motion of interstitial clusters provides a key element for microstructure morphology selection. In particular, it results in the formation of the void lattice in parallel orientation with the underlying crystal structure, in agreement with experimental observations. We also find that bcc and fcc void lattices develop in bcc and fcc crystals, respectively, while in hcp crystals, voids form ordered arrays parallel to basal planes. It is also predicted that a fcc void lattice is unstable, explaining the experimental difficulty for void lattice formation in fcc crystals.

DOI: 10.1103/PhysRevB.67.0641XX

PACS number(s): 61.80.Az, 61.72.Bb, 61.72.Cc, 61.72.Ji

I. INTRODUCTION

Extensive experimental observations on irradiated materials have systematically shown the existence of fully or partially ordered defect populations in materials under energetic particle irradiation, such as irradiation by ions, neutrons or electrons. Various types of defect microstructure (e.g., voids, precipitates, vacancy clusters, stacking fault tetrahedra, gas bubbles, and interstitial atom clusters) have been experimentally observed to be partially arranged in self-organized spatial patterns. Implantation of metals with energetic helium results in remarkable self-assembled bubble superlattices with wavelengths in the range of 5–8 nm. Ion and neutron irradiation, on the other hand, produce a wide variety of self-assembled three-dimensional defect walls and void lattices, with wavelengths that can be tailored in the range of tens to hundreds of nanometers.¹ Striking observations have shown complete spatial isomorphism between the periodic structure of defect distributions and that of the fundamental atomic lattice. These experimental observations are particularly true for the spatial ordering of bubble and void defect structures.^{2–7} An important aspect of void lattice formation in metals is the orientation of void patterns along crystallographic directions. Detailed and systematic observations of defect ordering under ion irradiated nickel and copper have shown the development of periodic defect walls.⁸ Formation of the walls of defect clusters in polycrystalline and single-crystalline Cu and Ni were observed at medium temperatures and high irradiation doses. The experimental observations of Jaeger and co-worker have clearly demonstrated strong anisotropic arrangements of stacking fault tetrahedra and vacancy type clusters in walls along the {100} planes of the fcc crystal lattice. Because of the equivalency between {100} planes, labyrinth structures were observed.⁹ These arrangements show a periodicity of 60 nm, with the walls having a thickness of less than half the periodicity length and defect-free zones are observed in between the walls. One of the significant observations is that the spatial wavelength is

rather insensitive to temperature, dose, and displacement damage rate.

Thermodynamic concepts of energy minimization were used to interpret void lattice structures in irradiated materials, and precipitate ordering during aging of alloys.¹⁰ However, the energy minima that are obtained do not correspond to the observed void lattice parameters or symmetries. In addition, the elastic interaction between voids is too weak to trigger morphological selection.¹¹ An important class of models, originating in the early approach of Foreman,¹² are based on the effect of the anisotropic diffusion of self-interstitial (SIA) atoms on voids. There are one and two-dimensional models of this type.^{13–15,11} In these models, the mechanism of void ordering is based on a detailed evaluation of SIA fluxes received by voids as a function of their spatial arrangement. The models predict that the growth rates of aligned voids are faster than those for isolated ones, which actually shrink. In the same spirit, other models have been proposed, which consider the interaction between interstitial loops and voids as the main selection mechanism of the void microstructure.¹⁶ This class of models favor equilibrium-type concepts rather than dynamical ones. They also require pre-existing random distributions of voids and point defects. They depend on defect mobility, but not on defect production rates or interactions. Furthermore, it is known that spatially uniform point defect and dislocation distributions may easily become unstable under irradiation.⁸ Hence, the resulting defect microstructure should also affect void distributions.

Recently, a coherent understanding of the spatial evolution of the microstructure, including void ordering, has been sought within the theoretical framework describing irradiation-induced self-organization of material defects.¹⁷ In this approach, rate equations describing the evolution of each relevant defect density are derived. These equations are based on the fundamental elements of defect dynamics, namely, point defect creation, recombination, and migration to the microstructure. Uniform solutions are searched, and their stability versus inhomogeneous perturbations studied.

Instability criteria that depend on kinetic rate coefficients, and thus on material parameters, may then be found.^{18–22} The combination of nonlinear interactions, bias, and mobility differences between several defect populations easily induces pattern forming instabilities. Similar to other pattern forming systems (e.g., chemical, hydrodynamic, etc.), the derivation of instability criteria through the linear stability analysis of uniform defect distributions is not sufficient to determine the spatial orientations of self-organized patterns. A nonlinear analysis of the post-bifurcation regime is required to establish the conditions for pattern symmetry and orientation. The selected microstructure crucially depends on nonlinear interactions between unstable spatial modes.²³ Furthermore, the microstructure symmetry and orientation may hinge on spatial anisotropies inherent to crystalline materials. In particular, it has been shown that loop and void patterns have parallel orientations with the directions of maximum cluster mobility.²²

In a series of papers, Walgraef and co-workers^{1,21,22,24,25} derived reaction-diffusion models for the coupled evolution of various families of defects involved in microstructure formation under irradiation. These models were analyzed from the point of view of nonlinear dynamics and pattern formation theory. They first considered point and line defects only, and the spatial ordering of vacancy loops. Then, in order to describe microstructure formation and evolution in general, they extended the dynamical model to include volume defects such as voids or stacking fault tetrahedra and discussed how the presence of such defects could affect microstructure evolution. The only mobile defects in this model are the point defects. They showed how different mobilities and bias in point defect evolution could trigger instabilities in uniform defect distributions and induce the formation of self-organized defect microstructure.²² Based on these theoretical approaches and on experimental findings, the following conditions appear to be necessary for the formation of ordered defect microstructure:

- (1) Direct formation of vacancy clusters by collision cascades;
- (2) preferential absorption of interstitials over vacancies at preexisting dislocations;
- (3) a degree of anisotropy influencing the evolution of clustered defects. This could either be a result of point defect diffusional anisotropy, or the anisotropic elastic interaction between defect clusters.

Recent molecular-dynamics computer simulations of collision cascades have shown that SIA clusters can also be directly produced in the neighborhood of cascades.²⁶ Glissile clusters of this type may be absorbed at void sinks, and implications of this phenomenon to swelling and other macroscopic phenomena have been recently discussed.^{1,27–31} It would thus be important to study the effects of glissile SIA clusters on the dynamics of microstructure formation in the framework of the dynamical approach described so far. The aim of this paper is to generalize the dynamical model introduced in Ref. 22 by incorporating the direct production of glissile clusters in collision cascades, and their subsequent dynamics. In Sec. II we introduce and discuss this generalized model and its uniform solutions. In Sec. III, we present

the linear stability analysis of uniform solutions and the onset of microstructure formation. We discuss microstructure selection in the weakly nonlinear regime and compare our results with experimental observations. Finally, conclusions are outlined in Sec. IV

II. THE DYNAMICAL MODEL

We generalize here our model,²² by explicitly accounting for glissile SIA clusters, which are directly produced in cascades and diffuse one dimensionally along close-packed crystallographic directions. Such clusters may be absorbed at immobile sinks such as network dislocations, vacancy or interstitial loops, voids, etc. They are characterized by a Burgers vector parallel to one of the close-packed directions of the crystal and we will consider the situation where the frequency of changing their Burgers vector direction during motion between sinks is equivalent in all motion directions, thus their populations along motion directions are equal. Glissile SIA clusters are divided into families characterized by their Burgers vector and represented by partial concentrations that satisfy different kinetic equations. With these restrictions, the model is then based on the following kinetic equations:

$$\begin{aligned}
 \partial_t c_i &= K(1 - \epsilon_i) - \alpha c_i c_v + D_i \nabla^2 c_i \\
 &\quad - D_i c_i (Z_{iN} \rho_N + Z_{iV} \rho_V + Z_{iI} \rho_I + Z_{iC} \rho_C), \\
 \partial_t c_v &= K(1 - \epsilon_v) - \alpha c_i c_v + D_v \nabla^2 c_v - D_v [Z_{vN} (c_v - \bar{c}_{vN}) \rho_N \\
 &\quad + Z_{vV} (c_v - \bar{c}_{vV}) \rho_V + Z_{vI} (c_v - \bar{c}_{vI}) \rho_I \\
 &\quad + Z_{vC} (c_v - \bar{c}_{vC}) \rho_C], \\
 \partial_t c_{gp} &= \epsilon_{gp} K - (D_g)_p \Pi_g^2 c_{gp} + (D_g)_p \nabla_p^2 c_{gp}, \\
 \partial_t \rho_I &= \left(\frac{2\pi N}{|\bar{b}|} \right) \left(\epsilon_s K + D_i Z_{iI} c_i - D_v Z_{vI} (c_v - \bar{c}_{vI}) \right. \\
 &\quad \left. + \sum_{p=1}^N a_p (D_g)_p Z_{gI} \Pi_g c_{gp} \right), \\
 \partial_t \rho_V &= \frac{1}{|\bar{b}| r_V^0} \left[\epsilon_v K - \rho_V \left(D_i Z_{iV} c_i - D_v Z_{vV} (c_v - \bar{c}_{vV}) \right. \right. \\
 &\quad \left. \left. + \sum_{p=1}^N a_p (D_g)_p Z_{gV} \Pi_g c_{gp} \right) \right], \\
 \partial_t \rho_C &= \frac{(4\pi N_c)^2}{\rho_C} [D_v Z_{vC} (c_v - \bar{c}_{vC}) - D_i Z_{iC} c_i] \\
 &\quad - \pi N_c \sum_{p=1}^N a_p (D_g)_p \Pi_g c_{gp}, \tag{1}
 \end{aligned}$$

where $\Pi_g^2 = (Z_{gN} \rho_N + Z_{gV} \rho_V + Z_{gI} \rho_I + Z_{gC} \rho_C)^2$ is the total sink strength for one-dimensional diffusing SIA clusters. Its

quadratic dependence in the defect densities is due to the fact that, in one dimension, the motion of a diffusing cluster is confined between two neighboring sinks, as discussed in Refs. 32 and 33. The notations are similar to the ones used in Ref. 22: c_v corresponds to the concentration of vacancies and c_i to SIA's, while the new variable c_g represents the concentration of glissile SIA clusters. ρ_N is the network dislocation density, ρ_v is the vacancy loop density, ρ_l is the sessile interstitial loop density and ρ_c is the void sink density ($\rho_c = 4\pi N_c R_c$ with N_c being the void number density and R_c begin the mean void radius). K is the displacement damage rate, $\epsilon_{gp}K$ and $\epsilon_s K$ are the glissile and sessile interstitial cluster production rates, respectively. p labels individual close-packed directions among the N present in the crystal (explicit examples will be considered later on), $\epsilon_i = \epsilon_s + \sum_{p=1}^N a_p \epsilon_{gp}$, and ϵ_v is the cascade collapse efficiency. α is the recombination coefficient, \vec{b} is the Burgers vector, r_v^0 is the mean vacancy loop (or cluster) radius, and Z_{\dots} are the bias factors (which may usually be approximated by $Z_{iN} = Z_{il} = Z_{iv} = 1 + B$ and $Z_{vI} = Z_{vN} = Z_{vV} = Z_{vC} = Z_{iC} = 1$, B being the excess network bias). \bar{c}_{vN} , \bar{c}_{vV} , \bar{c}_{vI} , and \bar{c}_{vC} are the concentrations of thermally emitted vacancies from network dislocations, vacancy and interstitial loops, and voids, respectively. $Z_{gN,V,I}$ are cross-section coefficients for absorbing glissile SIA clusters, and are proportional to the typical absorption distance for each type of sink. In particular, $Z_{gC} \approx (1/16\pi N_c)$. (Ref. 32) ($Z_{gN} \approx Z_{gV} \approx Z_{gI} \neq Z_{gC}$). $(D_g)_p$ is the diffusion coefficient of glissile SIA clusters along the p direction and a_p is the fraction of absorbed SIA in the p direction. Let us recall that the basic processes responsible for defect density evolution remain unchanged. Their net production rate results from the balance between displacement damage rate, responsible for the generation of Frenkel pairs, and loop production rates. Vacancy and interstitial loops are assumed to be produced directly by cascades, and their production rate is proportional to the corresponding cascade collapse efficiency. Point defects are annihilated through pair recombination or absorption at line (dislocations and loops) or volume (voids or bubbles) defects. The sink strengths for point defect absorption are $Z_{i\chi}\rho_\chi$ and $Z_{v\chi}\rho_\chi$ for interstitials and vacancies, respectively (χ representing the type of line or volume defect). The difference between $Z_{i\chi}$, $Z_{v\chi}$, and $Z_{g\chi}$ introduces new bias in defect evolution.

The main element in the present model is thus the presence of glissile SIA clusters, which has not been previously analyzed. SIA clusters are produced directly by a cascade effect and interact with all microstructural sinks in Eq. (1). For each sink, their absorption cross section is proportional to the mean radius and the sink density. Their motion is highly anisotropic, following well-defined crystallographic directions. These directions correspond, for example, to $\langle 111 \rangle$ directions in bcc lattices and $\langle 110 \rangle$ directions in fcc lattices.

A. Model equations in scaled variables

Let us first simplify model (1) on taking into account the equivalence of close-packed directions ($\epsilon_{gp} = \epsilon_g$, $(D_g)_n = D_g$, $a_n = a$) and on introducing the following scaling relations:

$$\lambda_v = D_v Z_{vN} \rho_N, \quad \bar{D}_v = D_v / \lambda_v, \quad \alpha / \lambda_v = \gamma,$$

$$P = \gamma K / \lambda_v,$$

$$\rho_{v,I,C}^* = \frac{\rho_{v,I,C}}{\rho_N}, \quad x_{i,v} = \gamma c_{i,v},$$

$$\bar{x}_{vN} \langle \bar{x}_{vV} \approx \bar{x}_{vI} \approx \bar{x}_{vC} = \bar{x}_{vL},$$

$$Z = \frac{Z_{gC}}{Z_{gN}}, \quad \mu = \frac{D_i}{D_v}, \quad \nu = \frac{D_g Z_{gN} \rho_N}{D_v}, \quad \tau = \lambda_v t,$$

$$\tau_I = \frac{b \alpha \rho_N}{2 \pi N D_v}, \quad \tau_V = b r_v^0 \rho_N \gamma, \quad \tau_C = \frac{\alpha \rho_N^2}{(4 \pi N_c)^2 D_v}. \quad (2)$$

It may then be written in dimensionless form, and the resulting dynamics is given by

$$\begin{aligned} \partial_\tau x_i &= P(1 - \epsilon_i) - x_i x_v + \mu \bar{D}_v \nabla^2 x_i \\ &\quad - \mu x_i [(1 + B)(1 + \rho_v^* + \rho_l^*) + \rho_c^*], \end{aligned}$$

$$\begin{aligned} \partial_\tau x_v &= P(1 - \epsilon_v) - \bar{x}_{vL} x_i x_v + \bar{D}_v \nabla^2 x_v \\ &\quad - (x_v - \bar{x}_{vL})(1 + \rho_v^* + \rho_l^* + \rho_c^*), \end{aligned}$$

$$\partial_t x_{gp} = \epsilon_g P - \nu x_{gp} (1 + \rho_v^* + \rho_l^* + Z \rho_c^*)^2 + \bar{D}_g \nabla_p^2 x_{gp},$$

$$\tau_I \partial_\tau \rho_l^* = \epsilon_s P + \mu (1 + B) x_i - (x_v - \bar{x}_{vL})$$

$$+ a \nu (1 + \rho_v^* + \rho_l^* + Z \rho_c^*) \sum_p x_{gp},$$

$$\begin{aligned} \tau_V \partial_\tau \rho_v^* &= \epsilon_v P - \rho_v^* \left(\mu (1 + B) x_i - (x_v - \bar{x}_{vL}) \right. \\ &\quad \left. + a \nu (1 + \rho_v^* + \rho_l^* + Z \rho_c^*) \sum_p x_{gp} \right), \end{aligned}$$

$$\begin{aligned} \tau_C \partial_\tau \rho_c^* &= \frac{1}{\rho_c^*} \left[(x_v - \bar{x}_{vL}) - \mu x_i \right. \\ &\quad \left. - a \nu (1 + \rho_v^* + \rho_l^* + Z \rho_c^*) \sum_p x_{gp} \right]. \quad (3) \end{aligned}$$

B. Uniform solutions

As discussed in Ref. 22, point defect densities evolve much more rapidly as compared to the microstructure, and may be adiabatically eliminated from the dynamics. Since glissile SIA clusters have also very high diffusivity, their dynamics will likewise be adiabatically eliminated. Their concentrations may thus be expressed as functions of dislocation, loop and void densities. In the case of uniform defect densities, one has, in the sink dominated regime ($\alpha \ll 1$).²²

$$\begin{aligned} (x_v^0 - \bar{x}_{vL}) &= \frac{P(1 - \epsilon_v) - \Delta}{A_0}, \\ x_i^0 &= \frac{P(1 - \epsilon_i)}{\mu(1 + B)B_0}, \\ x_{gp}^0 &= \frac{\epsilon_g P}{\nu C_0^2}, \end{aligned} \quad (4)$$

where $\Delta = \bar{x}_{vL} - \bar{x}_{vN} \approx \bar{x}_{vL}$, $A_0 = 1 + \rho_v^0 + \rho_l^0 + \rho_c^0$, $B_0 = 1 + \rho_v^0 + \rho_l^0 + \rho_c^0 / (1 + B)$, and $C_0 = 1 + \rho_v^0 + \rho_l^0 + Z\rho_c^0$.

Hence, the uniform steady states for point defect and SIA cluster densities are given by

$$\begin{aligned} \tau_l \partial_\tau \rho_l^0 &= \epsilon_s P + \frac{P(1 - \epsilon_i)}{B_0} - \frac{P(1 - \epsilon_v) - \Delta}{A_0} + \frac{Na\epsilon_g P}{C_0}, \\ \tau_v \partial_\tau \rho_v^0 &= \epsilon_v P - \left[\frac{P(1 - \epsilon_i)}{B_0} - \frac{P(1 - \epsilon_v) - \Delta}{A_0} + \frac{Na\epsilon_g P}{C_0} \right] \rho_v^0, \\ \tau_c \partial_\tau \rho_c^0 &= -\frac{1}{\rho_c^0} \left[\frac{P(1 - \epsilon_i)}{(1 + B)B_0} - \frac{P(1 - \epsilon_v) - \Delta}{A_0} + \frac{Na\epsilon_g P}{C_0} \right]. \end{aligned} \quad (5)$$

III. SPATIAL INSTABILITIES AND MICROSTRUCTURE FORMATION

The stability of uniform defect distributions may be studied through the linear evolution of small inhomogeneous per-

turbations. As shown in Ref. 22, point defect perturbations may be expressed as an expansion in powers of the loop density perturbations, and their Fourier transform may be written, in vectorial form, as

$$\begin{aligned} \delta \vec{x}_{\mathbf{q}} &= \sum_{n \geq 1} \int d\mathbf{k} \dots \int d\mathbf{k}_{n-1} (-1)^{(n)} \mathbf{D}_{\mathbf{q}, \dots, \mathbf{k}_{n-1}}^{(n)} \vec{T}_{\mathbf{q}} \\ &\times \delta \rho_{\mathbf{q}-\mathbf{k}} \dots \delta \rho_{\mathbf{k}_{n-1}} + \dots, \end{aligned} \quad (6)$$

where

$$\delta \vec{x}_{\mathbf{q}} = \begin{pmatrix} \delta x_{i,\mathbf{q}} \\ \delta x_{v,\mathbf{q}} \\ \delta x_{g_i,\mathbf{q}} \\ \dots \\ \delta x_{gN,\mathbf{q}} \end{pmatrix}, \quad (7)$$

$$\vec{T}_{\mathbf{q}} = \begin{pmatrix} \frac{P(1 - \epsilon_i)}{\mu(1 + B)B_0} \\ \frac{P(1 - \epsilon_v) - \Delta}{A_0} \\ \frac{a\epsilon_g P}{C_0} \\ \dots \\ \frac{a\epsilon_g P}{C_0} \end{pmatrix}, \quad (8)$$

$$\mathbf{D}_{\mathbf{q}, \dots, \mathbf{k}_{n-1}}^{(n)} = \begin{pmatrix} \frac{1}{B_q \dots B_{k_{n-1}}} & 0 & 0 & \dots \\ 0 & \frac{1}{A_q \dots A_{k_{n-1}}} & 0 & \dots \\ 0 & 0 & \frac{(2C_0)^n}{\nu^n C_{q1} \dots C_{k_{n-1}1}} & \dots \\ 0 & 0 & \dots & \frac{(2C_0)^n}{\nu^n C_{qN} \dots C_{k_{n-1}N}} \end{pmatrix}, \quad (9)$$

and

$$\delta \rho_{\mathbf{q}} = \rho^0 \delta \vec{\rho}_{\mathbf{q}} \quad (10)$$

with

$$\rho^0 = \begin{pmatrix} \rho_v^0 & \rho_l^0 & \frac{\rho_c^0}{1+B} \\ \rho_v^0 & \rho_l^0 & \rho_c^0 \\ \rho_v^0 & \rho_l^0 & 2Z\rho_c^0 \end{pmatrix} \quad (11)$$

and

$$\delta \vec{\rho}_{\mathbf{q}} = \begin{pmatrix} \delta \rho_{v\mathbf{q}} \\ \delta \rho_{l\mathbf{q}} \\ \delta \rho_{c\mathbf{q}} \end{pmatrix}. \quad (12)$$

Furthermore, $B_q = B_0 + q^2 \bar{D}_v / (1 + B)$, $A_q = A_0 + q^2 \bar{D}_v$, $C_{qp} = C_0 + q_p^2 D_g^*$, with $(D_g^* = \bar{D}_g / \sqrt{av})$, and

$$\begin{aligned} \delta x_i &= x_i - x_i^0, \quad \delta x_v = x_v - (x_v^0 - \bar{x}_{vL}), \quad \delta x_{gp} = x_{gp} - x_{gp}^0, \\ \delta \rho_v &= \frac{\rho_v^* - \rho_v^0}{\rho_v^0}, \quad \delta \rho_l = \frac{\rho_l^* - \rho_l^0}{\rho_l^0}, \quad \delta \rho_c = \frac{\rho_c^* - \rho_c^0}{\rho_c^0}, \end{aligned} \quad (13)$$

where x_i^0 , x_v^0 , ρ_v^0 , ρ_l^0 , and ρ_c^0 are the uniform defect densities.

This adiabatic elimination of point defect and SIA cluster densities leads thus to a reduction in the dynamics of sessile interstitial clusters, dislocation loops and void densities, which govern the evolution of the whole system. The evolution equations of nonuniform loop and void densities may then be cast in the following vectorial form:

$$\begin{aligned} \tau \partial_\tau \delta \vec{\rho}_q &= \mathbf{L} \delta \vec{\rho}_q + \mathbf{M} \delta \vec{x}_q + \int d\mathbf{k} \delta \vec{\rho}_{q-\mathbf{k}} \mathbf{N} \delta \vec{x}_k \\ &+ \int d\mathbf{k} \delta \vec{\rho}_{q-\mathbf{k}} \mathbf{P} \delta \vec{\rho}_k + \dots, \end{aligned} \quad (14)$$

where

$$\tau = \begin{pmatrix} \tau_v & 0 & 0 \\ 0 & \tau_l & 0 \\ 0 & 0 & \tau_c \end{pmatrix}, \quad (15)$$

$$\mathbf{L} = \begin{pmatrix} -\frac{\epsilon_v P}{\rho_v^0} & 0 & 0 \\ 0 & -\frac{(\epsilon_s P + \Gamma)}{\rho_l^0} & 0 \\ 0 & 0 & \frac{2}{\rho_c^0} \bar{\Gamma} \end{pmatrix}, \quad (16)$$

$$\mathbf{M} = \begin{pmatrix} -\mu(1+B) & 1 & -\nu C_0 & \dots & -\nu C_0 \\ \frac{\mu(1+B)}{\rho_l^0} & -\frac{1}{\rho_l^0} & \frac{\nu C_0}{\rho_l^0} & \dots & \frac{\nu C_0}{\rho_l^0} \\ -\frac{\mu}{\rho_c^0} & \frac{1}{\rho_c^0} & -\frac{\nu C_0}{\rho_c^0} & \dots & -\frac{\nu C_0}{\rho_c^0} \end{pmatrix}, \quad (17)$$

$$\mathbf{N} = \begin{pmatrix} -\mu(1+B) & 1 & -\nu C_0 & \dots & -\nu C_0 \\ 0 & 0 & \frac{\nu C_0}{\rho_l^0} & \dots & \frac{\nu C_0}{\rho_l^0} \\ \frac{\mu}{\rho_c^0} & -\frac{1}{\rho_c^0} & \frac{\nu C_0}{\rho_c^0} & \dots & \frac{\nu C_0}{\rho_c^0} \end{pmatrix} \quad (18)$$

and

$$\mathbf{P} = \begin{pmatrix} 0 & 0 & -\nu \\ 0 & 0 & \frac{\nu}{\rho_l^0} \\ 0 & 0 & -\frac{\bar{\Gamma}}{\rho_c^0} \end{pmatrix} \quad (19)$$

with

$$\begin{aligned} \Gamma &= \frac{P(1-\epsilon_i)}{B_0} - \frac{P(1-\epsilon_v) - \Delta}{A_0} + \frac{aN\epsilon_g P}{C_0}, \\ \bar{\Gamma} &= \frac{P(1-\epsilon_i)}{(1+B)B_0} - \frac{P(1-\epsilon_v) - \Delta}{A_0} + \frac{aN\epsilon_g P}{C_0}, \end{aligned}$$

and supplemented with equations (6).

A. The onset of spatial instability of the microstructure

In order to determine the possible development of spatial instability in the system, one has to know, in the first place, the evolution of the uniform loop and void defect densities, which may be evaluated through Eqs. (6) and (14).

Consider first the growth rate of the void density. It is easy to see that, when the net contribution of interstitials and SIA clusters to the void growth rate exceeds the net contribution of vacancies to the void growth rate, the asymptotic microstructure evolution is restricted to the evolution of dislocation loops only. Of course, due to the weak coupling between the loops and void densities, any spatial instability in loop densities will eventually induce transient structures in the void density. This condition is consistent with the experimental condition of irradiation at low temperatures (less than one-third of the melting point).

On the other hand, under conditions conducive for void growth (temperatures above one-third of the melting point), the situation is quite different, since a dimensional analysis of the evolution equations (5) shows that both loop and void densities increase first with time or irradiation dose, but may reach a steady state, thanks to the effect of the one-dimensional motion of glissile SIA clusters.³¹

The stability of uniform dislocation densities may be analyzed through the linear part of the evolution equation for their inhomogeneous perturbations. This evolution is obtained by combining Eqs. (6) and (14). Its linear part reads

$$\tau \partial_\tau \delta \vec{\rho}_q = [\mathbf{L} - \mathbf{M} \mathbf{D}_q \bar{T}_q \rho^0] \delta \vec{\rho}_q = \mathbf{\Omega}_q \delta \vec{\rho}_q, \quad (20)$$

where

$$\mathbf{\Omega}_q = \begin{bmatrix} -\frac{\epsilon_v P}{\rho_v^0} + \Lambda_q \rho_v^0 & \Lambda_q \rho_l^0 & \bar{\Lambda}_q \rho_c^0 \\ -\Lambda_q \frac{\rho_v^0}{\rho_l^0} & -\frac{(\epsilon_s P + \Gamma)}{\rho_l^0} - \Lambda_q & -\bar{\Lambda}_q \frac{\rho_c^0}{\rho_l^0} \\ \bar{\Lambda}_q \frac{\rho_v^0}{\rho_c^0} & \bar{\Lambda}_q \frac{\rho_l^0}{\rho_c^0} & \frac{2}{\rho_c^0} \bar{\Gamma} + \bar{\Lambda}_q \frac{1}{\rho_c^0} \end{bmatrix}, \quad (21)$$

where

$$\Lambda_q = \frac{P(1-\epsilon_i)}{B_0 B_q} - \frac{P(1-\epsilon_v) - \Delta}{A_0 A_q} + a \epsilon_g P \sum_p \frac{2Z\rho_C^0}{C_0 C_{qp}}, \quad (22)$$

$$\bar{\Lambda}_q = \frac{P(1-\epsilon_i)}{(1+B)B_0 B_q} - \frac{P(1-\epsilon_v) - \Delta}{A_0 A_q} + a \epsilon_g P \sum_p \frac{2Z\rho_C^0}{C_0 C_{qp}}, \quad (23)$$

$$\bar{\bar{\Lambda}}_q = \frac{P(1-\epsilon_i)}{(1+B)^2 B_0 B_q} - \frac{P(1-\epsilon_v) - \Delta}{A_0 A_q} + a \epsilon_g P \sum_p \frac{2Z\rho_C^0}{C_0 C_{qp}}. \quad (24)$$

The determination of the instability threshold is completely similar to the one made in Ref. 22. At the same level of approximation, one finds that the linear growth rate of Fourier modes of wave vector \vec{q} is proportional to

$$\omega_q \propto \frac{b-b_c}{b_c} - \xi_0^2 \left(\frac{q^2 - q_c^2}{q_c^2} \right)^2 + \xi_g^2 \sum_p \frac{1}{1 + D_\perp q_p^2}. \quad (25)$$

On writing this expression in unscaled variables, one finds that the bifurcation parameter b_c is given by

$$b_c = \frac{\rho_v^0}{1 + \rho_v^0 + \rho_l^0} \Big|_c = \frac{2\sqrt{\epsilon_v B}}{B + \bar{\epsilon} + \kappa \frac{B}{1+B}}, \quad (26)$$

where $\bar{\epsilon} = \epsilon_v - \epsilon_i + (\Delta/P)$ and $\kappa = \rho_c^0 / (1 + \rho_v^0 + \rho_l^0)$. Furthermore,

$$q_c^2 = \frac{1 + \rho_v^0 + \rho_l^0}{\bar{D}_v} \frac{B - \bar{\epsilon} - \kappa(2B + \bar{\epsilon})}{B + \bar{\epsilon} + \kappa \frac{B}{1+B}} \quad (27)$$

and

$$\xi_0^2 = \frac{(B - \bar{\epsilon})^2}{8B^2}, \quad \xi_g^2 = \frac{aZ\epsilon_g b_c^2 \rho_C^0}{\epsilon_v (1 + Z\kappa)^2}, \quad D_\perp = \frac{D_g^*}{C_0}. \quad (28)$$

ξ_0 and ξ_g characterize the set of unstable wave vectors beyond instability ($b > b_c$), and provide a linear selection mechanism for microstructures. In isotropic systems, a band of wave numbers, such that $q_c^2 [1 - \sqrt{(b-b_c)/\xi_0^2 b_c}] \times \langle q^2 \rangle [1 + \sqrt{(b-b_c)/\xi_0^2 b_c}]$ is unstable, and ξ_0 defines the width of this band at a given value of the bifurcation parameter b . For large ξ_0 , the unstable band is sharp and the wave number of the microstructure is expected to be close to q_c ; while for small ξ_0 , the unstable band is wide and the microstructure is expected to be less regular, with a high content of harmonics.

On the other hand, glissile cluster dynamics introduces new terms, proportional to ξ_g , which affect the linear selection of growing spatial modes. Effectively, ξ_g breaks the orientation degeneracy and favors the growth of modes with

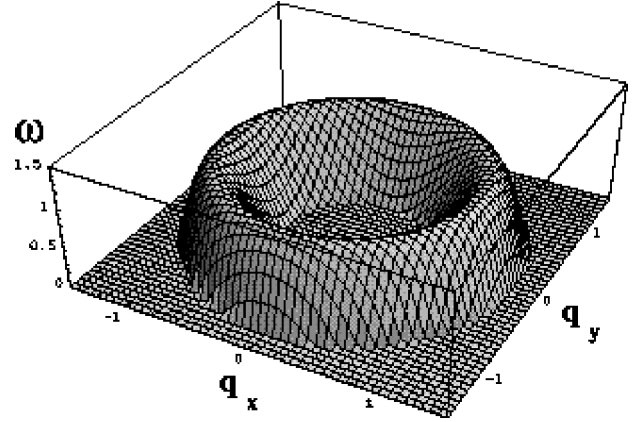


FIG. 1. Representation of positive growth rates, $\omega_q > 0$, in the (q_x, q_y) plane in the absence of glissile SIA clusters ($\epsilon_g = 0$), showing the orientation degeneracy of unstable modes ($b = 2b_c$, $q_c = 1$, $\xi_0 = 1$, $\xi_g = 0$).

wave vectors perpendicular to the directions of SIA motion. Their growth rates, and thus the anisotropy effect, increase both with SIA and void density. More precisely, the modes with maximum growth rate, which are expected to build the structure beyond instability, correspond to the wave vectors that maximize the total glissile cluster contribution $\sum_p 1/(1 + D_\perp q_p^2)$. Since this contribution depends on crystal structure, let us consider a few explicit examples.

For the simplest case of easy axis anisotropy, where glissile clusters move along the x direction, their diffusion contribution is $1/(1 + q_x^2 D_\perp)$. This implies that the fastest growing fluctuations are such that $q_x = 0$ or that their wave vectors are perpendicular to the x direction, as illustrated in Figs. 1–3. As a result, at least for the early stages of microstructure evolution, the domains of maximum defect density are

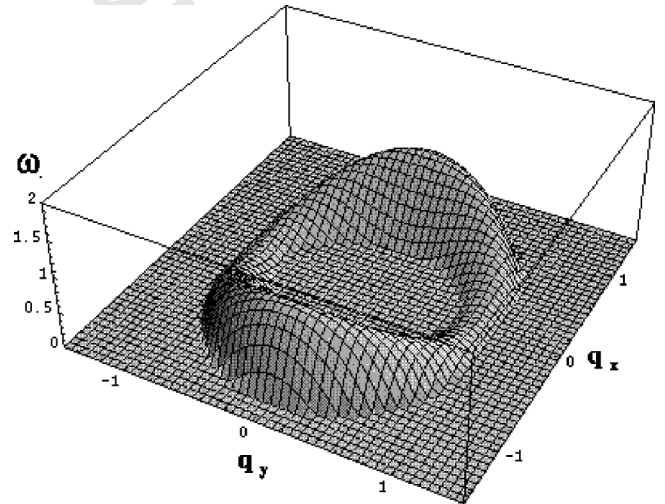


FIG. 2. Representation of positive growth rates, $\omega_q > 0$, in the (q_x, q_y) plane, in the presence of glissile SIA clusters ($\epsilon_g \neq 0$), with high mobility along the x axis. Fastest growing unstable modes have $q_x = 0$ and correspond to spatial modulations parallel to the high mobility axis of glissile clusters ($b = 2b_c$, $q_c = 1$, $\xi_0 = 1$, $\xi_g = 0.5$, $D_\perp = 4$).

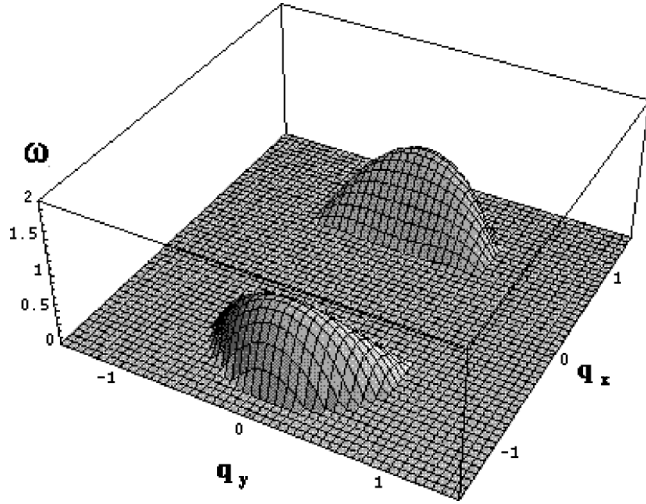


FIG. 3. Representation of positive growth rates, $\omega_q > 0$, in the (q_x, q_y) in the presence of glissile SIA clusters ($\epsilon_g \neq 0$), with high mobility along the x axis. The fastest growing unstable modes have $q_x = 0$ and correspond to spatial modulations parallel to the high mobility axis of glissile clusters ($b = 2b_c$, $q_c = 1$, $\xi_0 = 1$, $\xi_g = 1/\sqrt{2}$, $D_\perp = 4$).

expected to be parallel to the x direction, or to the direction of motion of the SIA clusters. Furthermore, the instability threshold is lowered to $b = b_c(1 - \xi_g^2)$. To know if the microstructure saturates in this orientation, one nevertheless needs to perform the post-bifurcation analysis. In the case of hcp crystals, glissile SIA clusters preferentially move on basal planes, or (x, y) planes, along close-packed directions, defined as the x direction and the directions making $2\pi/3$ angles with it. Their contribution to the linear growth rate of unstable modes is then

$$\frac{1}{1 + D_\perp q_x^2} + \frac{4}{4 + D_\perp (q_x + \sqrt{3}q_y)^2} + \frac{4}{4 + D_\perp (q_x - \sqrt{3}q_y)^2} = \frac{3 + 12D_\perp q_\perp^2 + 9D_\perp^2 q_\perp^4}{(1 + 6D_\perp q_\perp^2 + 9D_\perp^2 q_\perp^4 + D_\perp^3 q_1^2 q_2^2 q_3^2)}, \quad (29)$$

where $4q_\perp^2 = q_x^2 + q_y^2$ and $q_1 = q_x$, $q_2 = (q_x + \sqrt{3}q_y)/2$, $q_3 = (q_x - \sqrt{3}q_y)/2$. Hence, the modes that maximize the growth rate are such that $q_z = q_x = 0$, or $q_z = 0$ and $q_x = \pm\sqrt{3}q_y$ (see Fig. 4). These modes define a hcp structure in parallel orientation with the original lattice. The corresponding critical wavelength and instability thresholds are slightly modified as:

$$q_{hcp}^2 = q_c^2 \left[1 - \left(\frac{\xi_g}{\xi_0} \right)^2 \frac{12D_\perp q_c^2}{(4 + 3D_\perp q_c^2)^2} + O\left(\frac{\xi_g^4}{\xi_0^4} \right) \right],$$

$$b_{hcp} = b_c \left\{ 1 - \xi_g^2 \left[\frac{12 + 3D_\perp q_c^2}{4 + 3D_\perp q_c^2} + O\left(\frac{\xi_g^2}{\xi_0^2} \right) \right] \right\}. \quad (30)$$

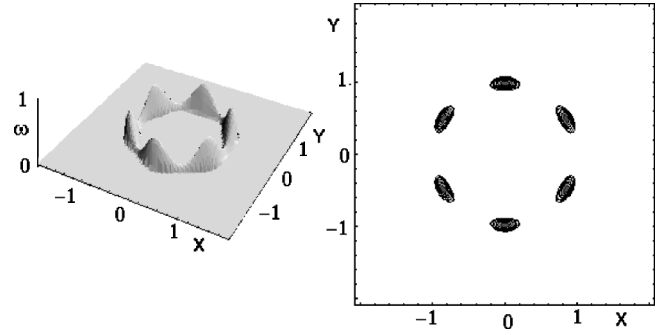


FIG. 4. Representation of positive growth rates, $\omega_q > 0$, and its maxima, in the $(q_x = X, q_y = Y)$ plane, in the presence of glissile SIA clusters ($\epsilon_g \neq 0$), with high mobility along the close-packed direction of a hcp lattice. The fastest growing unstable modes correspond to spatial modulations parallel to the high mobility axis of glissile clusters ($b = b_c$, $q_c = 1$, $\xi_0 = 2$, $\xi_g = 1$, $D_\perp = 5$).

For bcc crystals, the close-packed directions are the $\langle 111 \rangle$, $\langle 1\bar{1}1 \rangle$, $\langle 11\bar{1} \rangle$, and $\langle 1\bar{1}\bar{1} \rangle$ directions and the glissile clusters contribution to the linear growth rate is

$$\frac{1}{1 + D_\perp (q_x + q_y + q_z)^2} + \frac{1}{1 + D_\perp (q_x - q_y + q_z)^2} + \frac{1}{1 + D_\perp (q_x + q_y - q_z)^2} + \frac{1}{1 + D_\perp (q_x - q_y - q_z)^2}. \quad (31)$$

This expression is maximum for the six pairs of wave vectors that precisely define a bcc lattice in parallel orientation with the original one ($(q_x = 0, q_z = \pm q_y = \pm q)$, $(q_y = 0, q_z = \pm q_x = \pm q)$, $(q_z = 0, q_x = \pm q_y = \pm q)$) (see Fig. 5).

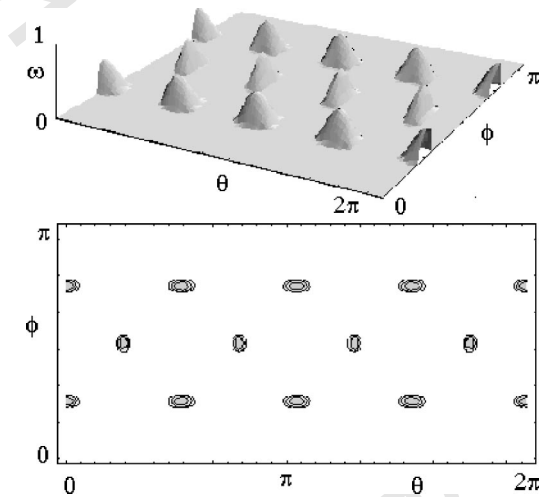


FIG. 5. Representation of the growth rate, $\omega_{q_c} > 0$, of critical modes, and its maxima, as a function of orientation, i.e., in the $(\theta, \phi, q_x = q_c \cos \theta \sin \phi, q_y = q_c \sin \theta \sin \phi, q_z = q_c \cos \phi)$ plane, in the presence of glissile SIA clusters ($\epsilon_g \neq 0$), with high mobility along the close-packed direction of a bcc lattice. The fastest growing unstable modes correspond to spatial modulations parallel to the high mobility axis of glissile clusters, which generate a bcc microstructure in parallel orientation with the crystal lattice ($b = b_c$, $q_c = 1$, $\xi_0 = 2$, $\xi_g = 1$, $D_\perp = 5$).

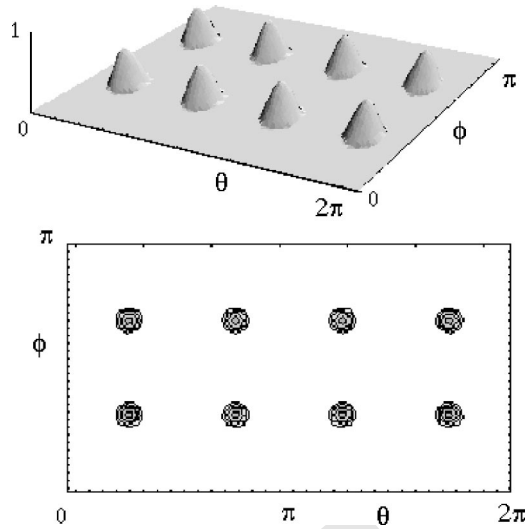


FIG. 6. Representation of the growth rate, $\omega_{qc} > 0$, of critical modes, and its maxima, as a function of orientation, i.e., in the $(\theta, \phi, q_x = q_c \cos \theta \sin \phi, q_y = q_c \sin \theta \sin \phi, q_z = q_c \cos \phi)$ plane, in the presence of glissile SIA clusters ($\epsilon_g \neq 0$), with high mobility along the close-packed direction of a fcc lattice. The fastest growing unstable modes correspond to spatial modulations parallel to the high mobility axis of glissile clusters, which generate a fcc microstructure in parallel orientation with the crystal lattice ($b = b_c, q_c = 1, \xi_0 = 2, \xi_g = 1, D_\perp = 5$).

The corresponding critical wavelength and instability thresholds are also slightly modified, and

$$q_{bcc}^2 = q_c^2 \left[1 - \left(\frac{\xi_g}{\xi_0} \right)^2 \frac{4D_\perp q_c^2}{(1 + 4D_\perp q_c^2)^2} + O\left(\frac{\xi_g^4}{\xi_0^4} \right) \right],$$

$$b_{bcc} = b_c \left[1 - 2\xi_g^2 \left(\frac{2 + 4D_\perp q_c^2}{1 + 4D_\perp q_c^2} + O\left(\frac{\xi_g^2}{\xi_0^2} \right) \right) \right]. \quad (32)$$

For fcc crystals, the close-packed directions are the $\langle 110 \rangle$, $\langle 1\bar{1}0 \rangle$, $\langle 101 \rangle$, $\langle 10\bar{1} \rangle$, $\langle 011 \rangle$, and $\langle 0\bar{1}1 \rangle$ directions and the glissile clusters contribution to the linear growth rate is

$$\frac{1}{1 + D_\perp (q_x + q_y)^2} + \frac{1}{1 + D_\perp (q_x - q_y)^2} + \frac{1}{1 + D_\perp (q_y - q_z)^2}$$

$$+ \frac{1}{1 + D_\perp (q_y + q_z)^2} + \frac{1}{1 + D_\perp (q_x + q_z)^2} + \frac{1}{1 + D_\perp (q_x - q_z)^2}. \quad (33)$$

In this case also, this expression is maximum for the four pairs of wave vectors that precisely define a fcc lattice in parallel orientation with the original one ($q_x = \pm q_z = \pm q_y = \pm q$) (see Fig. 6). The corresponding critical wavelength and instability thresholds are modified as follows:

$$q_{fcc}^2 = q_c^2 \left[1 - \left(\frac{\xi_g}{\xi_0} \right)^2 \frac{6D_\perp q_c^2}{(1 + 4D_\perp q_c^2)^2} + O\left(\frac{\xi_g^4}{\xi_0^4} \right) \right],$$

$$b_{fcc} = b_c \left\{ 1 - 3\xi_g^2 \left[\frac{2 + 4D_\perp q_c^2}{1 + 4D_\perp q_c^2} + O\left(\frac{\xi_g^2}{\xi_0^2} \right) \right] \right\}. \quad (34)$$

Hence, the one-dimensional motion of SIA glissile clusters provides a linear selection mechanism, favoring the growth of structures that are in parallel orientation with the host lattice. One has now to check whether or not these structures are stable in the nonlinear domain beyond the instability.

B. Microstructure selection in the weakly nonlinear regime

Once again, we follow the method used in Ref. 22, which is based on the adiabatic elimination of fast relaxing variables. In a first step, point defect densities have been expressed as series expansions in powers of void and loop densities. Furthermore, as discussed in Ref. 22, $\tau_C, \tau_I \gg \tau_V$. Hence, interstitial loop and void densities evolve on shorter time scales than vacancy loop density, and may be expressed as linear combinations of the eigenmodes of the linear evolution matrix. This leads to the following relations that express how they are linked to the vacancy loop density:

$$\delta\rho_{Iq} \propto -\frac{\epsilon_v}{\rho_V \epsilon_i} \delta\rho_{Vq}, \quad \delta\rho_{Cq}(\epsilon_g) \propto \delta\rho_{Vq}. \quad (35)$$

The fact that $\tau_C \gg \tau_I \gg \tau_V$ also implies that the elements of the matrices \mathbf{M} and \mathbf{N} are such that their lower components decrease with time or dose, and that the dynamics remains driven by the vacancy loops. For weak deviations from the uniform density, and at leading order in $\epsilon = (b - b_c)/b_c$ and $(q - q_c)/q_c$, the vacancy loop density plays thus the role of the order-parameter-like variable of the system. According to the general methods of nonlinear dynamics and instability theory, its dynamics may be expressed, in Fourier space, as a power-series expansion “in the manner of Landau.”²³ Close to the instability point, in the weakly nonlinear regime, it may be limited to cubic nonlinearities, and is given by

$$\tau_0 \partial_\tau \delta\rho_{Vq} = \omega_q \delta\rho_{Vq} + \int dk v_{qc} \delta\rho_{Vq-k} \delta\rho_{Vk}$$

$$+ \int dk \int dk_1 u_{qc} \delta\rho_{Vq-k} \delta\rho_{Vk-k_1} \delta\rho_{Vk_1}, \quad (36)$$

where the linear growth rate ω_q is given in Eq. (25). At this level of approximation, the other constants, v_{qc} and u_{qc} , calculated in Ref. 22, in the absence of SIA clusters, are only modified by small corrections proportional to ϵ_g/C_0 .

Equation (36) has the generic structure of order-parameter equations describing reaction-diffusion systems close to a pattern forming instability of the Turing type. It allows one to analyze pattern selection and stability. It is now well known²³ that, in three-dimensional systems, this equation admits, near threshold, and for scalar nonlinear interactions between dynamical modes, which is the case here, stable solutions corresponding to hcp and bcc lattices. fcc solutions are only marginally stable and planar arrays may develop well beyond threshold. These structures are stable in finite do-

mains around the instability, and the width of these domains is proportional to the intensity of the nonlinear dynamical couplings.²³ As a result, the linearly selected structures are compatible with the weakly nonlinear dynamics that governs the system beyond instability, in agreement with experimental observations. Furthermore, a very natural difference between the dynamics of void lattice formation in bcc and fcc crystals appears in our description. Effectively, bcc lattices appear through a subcritical bifurcation or first-order-like transition, and are dynamically stable, while fcc lattices appear supercritically (cf. the Appendix), and are only marginally stable. As a result, the bcc structures grow and reach steady state on much shorter time scales and are much more robust than the fcc structures, which develop long-lived, long-range perturbations. Furthermore, the SIA density is much lower in the fcc materials than in the bcc ones, which strongly reduces the anisotropy effect in the first ones. This aspect may explain the experimental difficulty in forming fcc void lattices.

In summary, glissile SIA clusters only weakly affect instability threshold, but strongly affect the symmetry and orientation of the microstructure. The selected microstructure has its domains of high defect (especially void) density oriented parallel to the directions, or planes, of high cluster mobility. In three-dimensional crystals, this results in a microstructure in parallel orientation with the underlying lattice. However, the stability of the microstructure may vary, according to its symmetry. For example, the hcp and bcc structures may appear subcritically and are stable, while the fcc structures are supercritical and are only marginally stable. At sufficiently high irradiation dose, these structures may become unstable and disappear in favor of planar wall arrangements.

IV. CONCLUSIONS

In this paper, we extend our previous analysis of microstructure formation and evolution in irradiated metals and alloys, to the case where glissile SIA clusters are formed by cascade effect and participate in the dynamics. Hence a dynamical model has been derived, based on the coupled evolution of three mobile defect populations, point defects and SIA clusters, and three immobile ones, vacancy and interstitial loops and voids. Point defects are assumed to diffuse isotropically in the crystal, while SIA clusters move on close-packed directions or planes of the host crystal.

In particular, we find that the presence of glissile SIA clusters only slightly affects critical values of the bifurcation parameter and wavelength. These quantities are sensitive to the void density that decreases the instability threshold and wavelength. Furthermore, the microstructure spatial instability originates from vacancy cluster dynamics, as in our previous model. However, in agreement with earlier proposals,¹² the anisotropic mobility of SIA clusters is an essential element of the selection of the microstructure, since it lifts the orientation degeneracy of unstable modes. We find that the high defect mobility along close-packed directions results in the alignment of the microstructure pattern with the host crystal lattice. This finding is not obvious, since, in reaction-

diffusion dynamics, net anisotropy effects result not only from the anisotropy of diffusion coefficients, but also from nonlinear couplings between the different dynamical variables of the system.²³ The instability may be enhanced or reduced along specific directions, which are not necessarily the high mobility ones. In the present case, the resulting anisotropy is determined by the fact that, close to the instability, the behavior of the system is governed by vacancy cluster dynamics. This leads to a series of results that are in good agreement with experimental observations. For example, bcc and fcc void lattices should develop in bcc and fcc crystals, while in HCP crystals, voids should be ordered parallel to the basal planes. Furthermore, our weakly nonlinear analysis predicts the instability of fcc microstructure, and this effect, coupled with the low observed SIA density in fcc crystals, could be related to the experimental difficulty for such lattices to form, in comparison with the easily obtained bcc ones. One should also note that the importance of this selection mechanism depends on D_{\perp} , which decreases for increasing void density. Hence, a less regular void microstructure may be expected at high void density.

In summary, we find that the incorporation of glissile SIA clusters, with their particular anisotropic motion, in our kinetic rate theory model confirms their essential role in determining the void lattice orientation and symmetry, and consistently reproduces experimentally observed microstructure selection and stability.

ACKNOWLEDGMENTS

Research was supported by the U.S. Department of Energy, Office of Fusion Energy, through Grant No. DE-FG03-98ER54500 and DOE Grant No. DE-FG03-01ER54626 with UCLA. D.W. was supported by the Belgian National Fund for Scientific Research. Fruitful discussions with S. Golubov are also gratefully acknowledged.

APPENDIX

The order-parameter-like variable $\delta\rho_V$ may be written, in the case of fcc lattices, as $\delta\rho_V = \sum_{i=1}^4 (A_i \exp i\vec{q}_i \vec{r} + A_i^* \exp -i\vec{q}_i \vec{r})$, where the \vec{q}_i vectors are defined as ($q_x = \pm q_z = \pm q_y = \pm q_{fcc}$). The corresponding amplitude equations may be derived from the order-parameter dynamics (36) and with appropriate scalings, can be written as

$$\dot{A}_1 = \left[\frac{b-b_c}{b_c} + 4(\vec{q}_1 \vec{V})^2 \right] A_1 - A_1 (|A_1|^2 + 2|A_2|^2 + 2|A_3|^2 + 2|A_4|^2) - A_2 A_3 A_4^*,$$

$$\dot{A}_2 = \left[\frac{b-b_c}{b_c} + 4(\vec{q}_2 \vec{V})^2 \right] A_2 - A_2 (|A_2|^2 + 2|A_1|^2 + 2|A_3|^2 + 2|A_4|^2) - A_1 A_4 A_3^*,$$

$$\begin{aligned}\dot{A}_3 &= \left[\frac{b-b_c}{b_c} + 4(\vec{q}_3 \vec{\nabla})^2 \right] A_3 - A_3(|A_3|^2 + 2|A_1|^2 + 2|A_2|^2 \\ &\quad + 2|A_4|^2) - A_1 A_4 A_2^*, \\ \dot{A}_4 &= \left[\frac{b-b_c}{b_c} + 4(\vec{q}_4 \vec{\nabla})^2 \right] A_4 - A_4(|A_4|^2 + 2|A_1|^2 + 2|A_3|^2 \\ &\quad + 2|A_2|^2) - A_2 A_3 A_1^*.\end{aligned}\quad (\text{A1})$$

Since the \vec{q}_i vectors do not form equilateral triangles, there is no contribution from quadratic nonlinearities to the dynamics, and the bifurcation is thus supercritical. Furthermore, there is an extra contribution to the cubic nonlinearity, since the \vec{q}_i vectors satisfy the condition $\vec{q}_1 + \vec{q}_4 - \vec{q}_3 - \vec{q}_2 = 0$. For symmetry reasons, one may expect uniform steady state solutions of the type $A_i = R \exp i\Phi_i$, such that

$$\begin{aligned}0 &= \left(\frac{b-b_c}{b_c} \right) R - 7R^3 - R^3 \cos \Phi_0, \\ 0 &= R^2 \sin \Phi_0.\end{aligned}\quad (\text{A2})$$

where $\Phi_0 = \Phi_1 + \Phi_4 - \Phi_2 - \Phi_3$. A linear stability analysis shows that, from the two solutions, $\Phi_0 = 0, R = R_0 = \sqrt{(b-b_c)/8b_c}$ and $\Phi_0 = \pi, R = R_\pi = \sqrt{(b-b_c)/6b_c}$, only the latter is stable. The stability of this solution versus uniform amplitude perturbations, $a_i (A_i = R_\pi + a_i)$, is studied through their linear evolution equations, which may be written as

$$\dot{a}_i = - \left(\frac{b-b_c}{2b_c} \right) \sum_{j=1}^4 a_j. \quad (\text{A3})$$

The roots of the corresponding evolution matrix are $\omega = -2[(b-b_c)/b_c]$ and $\omega = 0$. As a result, uniform fcc structures are marginally unstable. Although Φ_0 and $\sum_i |A_i|$ are stable modes (the corresponding eigenvalues are finite negative), the marginally unstable ones are the amplitude and phase differences $|A_i| - |A_j|$ and $\Phi_i - \Phi_j$. Furthermore, if one considers spatially dependent amplitude equations, it is easy to see that the marginally unstable modes may develop long-ranged spatial fluctuations, which lead to long-lived deformations or distortions of the lattice structure.

¹N.M. Ghoniem, D. Walgraef, and S. Zinkle, *J. Comp. Aided Mat. Design*, **8**, 1 (2002).

²S. Sass and B.L. Eyre, *Philos. Mag.* **27**, 1447 (1973).

³P.B. Johnson, D.J. Mazey, and J.H. Evans, *Radiat. Eff.* **78**, 147 (1983).

⁴J.H. Evans, *Nature (London)* **29**, 403 (1971); *Radiat. Eff.* **10**, 55 (1971).

⁵D.J. Mazey and J.H. Evans, *J. Nucl. Mater.* **138**, 16 (1986).

⁶G.L. Kulcinski, J.L. Brimhall, and H.E. Kissinger, in *Proceedings of the 1971 International Conference on Radiation-Induced Voids in Metals, Albany, 1971* (USAEC, Washington, DC, 1972), p. 465.

⁷F.W. Wiffen, in *Proceedings of the International Conference on Radiation-Induced Voids in Metals* (Ref. 6), p. 386.

⁸W. Jaeger, P. Ehrhart, and W. Schilling, *Solid State Phenom.* **3-4**, 297 (1988); *Radiat. Eff. Defects Solids* **113**, 201 (1990).

⁹W. Jaeger and H. Trinkaus, *J. Nucl. Mater.* **205**, 394 (1993).

¹⁰E. Johnson and L.T. Chadderton, *Radiat. Eff.* **79**, 183 (1983).

¹¹J.H. Evans, in *Patterns, Defects and Materials Instabilities*, edited by D. Walgraef and N.M. Ghoniem, (Kluwer, Dordrecht, 1990), pp. 347–370.

¹²A.J.E. Foreman, *AERE Reports* 7135, 1972 (unpublished).

¹³C.H. Woo and W. Frank, *J. Nucl. Mater.* **137**, 7 (1985); **140**, 214 (1986); **148**, 121 (1987); **206**, 170 (1993).

¹⁴J.H. Evans, *J. Nucl. Mater.* **119**, 180 (1983).

¹⁵J.H. Evans, *J. Nucl. Mater.* **132**, 147 (1985).

¹⁶V.I. Dubinko, A.V. Tur, A.A. Turkin, and V.V. Yanovsky, *J. Nucl. Mater.* **161**, 57 (1989).

¹⁷K. Krishan, *Nature (London)* **287**, 420 (1980).

¹⁸K. Krishan, *Solid State Phenom.* **3-4**, 267 (1988).

¹⁹S.M. Murphy, *Europhys. Lett.* **3**, 1267 (1987).

²⁰E.A. Koptelov and A.A. Semenov, *J. Nucl. Mater.* **160**, 253 (1988).

²¹D. Walgraef and N.M. Ghoniem, *Phys. Rev. B* **39**, 8867 (1989).

²²D. Walgraef, J. Lauzeral, and N.M. Ghoniem, *Phys. Rev. B* **53**, 14 782 (1996).

²³D. Walgraef, *Spatio-Temporal Pattern Formation* (Springer-Verlag, New York, 1996).

²⁴N.M. Ghoniem and D. Walgraef, *Modell. Simul. Mater. Sci. Eng.* **1**, 569 (1993).

²⁵D. Walgraef and N.M. Ghoniem, *Phys. Rev. B* **52**, 3951 (1995).

²⁶T. Diaz de la Rubia, R.S. Averback, H. Hsieh, and R. Benedek, *J. Mater. Res.* **4**, 579 (1989).

²⁷S.J. Zinkle and B.N. Singh, *J. Nucl. Mater.* **199**, 173 (1993).

²⁸C.H. Woo, A.A. Semenov, and B.N. Singh, *J. Nucl. Mater.* **206**, 170 (1993).

²⁹C.H. Woo and B.N. Singh, *Philos. Mag. A* **65**, 889 (1992).

³⁰B.N. Singh and A.J. Foreman, *Philos. Mag. A* **66**, 975 (1992).

³¹S.I. Golubov, B.N. Singh, and H. Trinkaus, *J. Nucl. Mater.* **276**, 78 (2000).

³²B.N. Singh, S.I. Golubov, H. Trinkaus, A. Serra, Yu.N. Osetsky, and A.V. Barashev, *J. Nucl. Mater.* **251**, 107 (1997).

³³S.L. Dudarev, *Phys. Rev. B* **62**, 9325 (2000).